Non-autonomous cell redox-pairs dictate niche homeostasis in multi-lineage stem populations

Olivia Majhi[1], Aishwarya Chhatre[1,2], Tanvi Chaudhary[1] and Devanjan Sinha[1#]

[1]Department of Zoology, Institute of Science, Banaras Hindu University, Varanasi, Uttar Pradesh, India

[2]Present address: Biological Research Centre, Institute of Genetics, Eötvös Loránd Research Network (ELKH), Szeged, Hungary

[#]To whom correspondence should be addressed:

Address for correspondence:
Dr. Devanjan Sinha,
Department of Zoology,
Institute of Science,
Banaras Hindu University,
Varanasi – 221005,
Uttar Pradesh, India
India
Email: devanjan@bhu.ac.in

Abstract

Reactive oxygen species (ROS), predominantly derived from mitochondrial respiratory complexes, have evolved as key molecules influencing cell fate decisions like maintenance and differentiation. These redox-dependent events are mainly considered to be cell intrinsic in nature, on contrary our observations indicate involvement of these oxygen-derived entities as intercellular communicating agents. In multi-lineage *Drosophila* germline, neighbouring Germline Stem Cells (GSCs) and Cystic Stem Cells (CySCs) maintain differential redox thresholds where CySCs by virtue of their higher redox-state regulate physiological ROS levels of germline. Disruption of the intercellular redox equilibrium between the two adjoining stem cell populations results in deregulated niche architecture and loss of GSCs, which was mainly attributed to loss of contact-based receptions and uncontrolled CySC proliferation due to ROS-mediated activation of self-renewing signals. Our observations hint towards the crucial role of intercellular redox gradients originating from somatic progenitors, CySCs in niche stability where they function not only as a source of their own maintenance cues but also serve as non-autonomous redox moderators of germline immortality. Our findings underscore the complexity of niche homeostasis and predicate the importance of intercellular redox communication in understanding stem cell microenvironments.

52 **Introduction**

53 Studies from the past few decades have shown the apparent role of ROS in influencing
54 various biological processes[1-3]. Generally, the sources of ROS are compartmentalized
55 in co-occurrence with their targets mediating important signalling events[4].
56 Mitochondria, a major source of oxidant species[5,6], localize dynamically towards
57 nucleus, effecting oxidation induced reshaping of gene expression profiles[7]. Localized
58 ROS production are contributed by NADH oxidases distributed across different cellular
59 regions[8]. Intracellular hydrogen peroxide gradients maintained by thioredoxin system
60 allow intercompartmental exchanges among endoplasmic reticulum (ER),
61 mitochondria and peroxisomes[9-11].

62 The process of redox relays is conserved and plays a fundamental role in self-renewal
63 and differentiation of stem cell populations[12]. Stem cells whether embryonic or adult
64 maintain a low redox profile, characterized by subdued mitochondrial respiration[13-17].
65 Levels of ROS are tightly regulated and elevated amounts promote early differentiation
66 and atypical stem cell behaviour[18]. However, leading evidences suggest that many
67 transcription factors require oxidative environment for maintenance of pluripotent
68 states. For instance, physiological ROS levels play a crucial role in genome
69 maintenance of embryonic stem cells[13]. Multipotent hematopoietic progenitors and
70 neural stem cells require relatively high baseline redox for their maintenance[14,16,19].
71 Suppression of Nox system or mitochondrial ROS compromises the maintenance of
72 these self-renewing populations and promote their differentiation or death[18]. These
73 evidences point towards essentiality of a perfectly tuned redox state for balancing the
74 pluripotent and differentiated states. But how the stem cells harmonize their redox
75 potential by possessing a restrained oxidant system is not very clear.

76 We addressed this fundamental question in multi-stem cell lineage-based niche
77 architecture in *Drosophila* testis. The testicular stem cell niche is composed of a
78 central cluster of somatic cells called the hub which contacts eight to eleven GSCs
79 arranged in a round array[20,21]. A pair of cystic stem cells (CySCs) originating the
80 somatic lineage cyst cells, enclose each GSC and make their independent
81 connections with the hub and GSCs via adherens junctions[22-26]. The hub cells secrete
82 Unpaired family of cytokines that defines niche occupancy and self-renewal of both
83 GSCs and CySCs through Jak-Stat signalling[27,28]. CySCs also repress GSC

differentiation by suppressing transcription of bag-of-marbles (Bam)[29,30]. Concerted asymmetric division of both GSC and CySC is essential for proper cyst formation[31]. A developing cyst contains a dividing and differentiating gonialblast encircled by cyst cells that provide nourishment to developing spermatids[32,33]. However, the maintenance of GSCs in the spatially controlled microenvironment is still not very clear.

We found the existence of a perfectly balanced redox differential between GSC and CySC essential for niche homeostasis. CySCs by virtue of their higher redox threshold and clustering of mitochondria at GSC-CySC interface, generate an intercellular redox gradient that maintain physiological ROS levels in GSCs. Alterations in CySC redox state affected self-renewal and differentiation propensities of the GSCs. Intercellular redox-imbalance induced niche disequilibrium through precocious differentiation of GSCs and deregulated CySC proliferation, due to activation of pro-proliferative transductions and loss of cell-cell contact signalling. Our results in multi-stem cell lineage-based germline system indicate a nuanced division of labour where a higher redox state in CySCs not only maintains their self-renewing processes but also non-autonomously foster GSCs maintenance.

Results

Redox state of GSC is maintained by asymmetric distribution of CySC mitochondria

The apical region of the Drosophila testis incorporates a cluster of differentiated cells the hub surrounded by GSCs in a rosette arrangement with each GSC being enclosed by two CySCs (Fig. 1A). The mitochondria morphology and distribution in this cluster was checked by immunostaining ATP5A subunit of mitochondrial ATPase. We observed fragmented mitochondria in Vasa^{+} GSCs as compared to a fused organization in Traffic jam (Tj)$^{+}$ CySCs (Fig. 1B#, C, D). Distribution profiles of mitochondria showed its higher propensity to overlap with Tj, indicating CySCs to be a mitochondria dense region compared to GSC (Fig. 1F); and its mitochondria to be predominantly clustered near the GSC-CySC boundary, illustrated by intensity profile (Fig. S1A’’’) and X-Z and Y-Z sectioning (Fig. S1B-B’). The ATP5A labelling

overlapped with *TFAM-GFP*, a mitochondrial transcription factor[34], further confirming the patterning observed between these two stem cell populations (Fig. S1C').

Mitochondria localization near the GSC-CySC boundary, together with its dispersion pattern was in accordance with the intensity variance of ROS reporter line *gstD1-GFP* [35] at the niche (Fig. 1H and S1D-D'). The redox gradient intensifies at the Tj-Vasa boundary and then gradually diffuses into Vasa^{+} GSCs, suggesting an establishment of GSC redox state through CySCs (Fig. 1Q; *left panel*). A GSC intrinsic oxidative environment should have resulted in a constant continuum of *gstD1*-GFP intensity across the Vasa-stained structure. We confirmed the greater ROS gradient at the GSC-CySC interface by 2D-Plot profile of Vasa, Tj and *gstD1*-GFP across the different cell types (Fig. S1E).

To affirm the role of CySC in influencing GSC redox state, we asked if disrupting dismutases in CySCs would influence the redox state of GSCs. We depleted the expression of superoxide dismutase 1 (Sod1) in CySCs and early differentiating cyst cells using *Tj-Gal4* driver (*Tj>Sod1i*). Higher CySC redox state resulted in corresponding increase in GSC ROS profile, as indicated by a greater degree gstD1-GFP intensity and DHE fluorescence at the Vasa-gstD1GFP (V∩G) intersection (Fig. 1K, P, R and S1F), suggesting non-autonomous maintenance of GSC redox gradient by CySCs (Fig. 1Q; *right panel*). The surge in GSC ROS levels upon lowering of antioxidant defences in CySCs, was additionally confirmed through enhanced Vasa:*gstD1*-GFP colocalization intensities in *Sod1i* populations (MCC^{mean} = 0.482) with respect of controls (MCC^{mean} = 0.276) (Fig. 1S). These observations hinted towards a potential role of CySCs and its GSC polarized mitochondria in elevating the cellular ROS gradient at the interface between two stem cell populations.

Balanced CySC redox profile is crucial for its proliferation and GSC maintenance

Along with the shift in the redox gradient, we observed that high ROS in *Tj>Sod1i* had a striking effect on the increase in DAPI^{+}-nuclei at the tip of testis (Fig. 1G and L). This overcrowding was attributed to an increase in number and positional shift in Tj^{+} CySCs and early differentiating cyst cells (Fig. 2A', B' and E). The enhancement in the number

146 of CySCs was also reflected by ~2-fold change in Zfh1^{+} cells (Fig. 2F). Vasa^{+} cells
147 flanking the hub however, substantially reduced in number (Fig. 2C''-D'' and G), which
148 was validated through lower detectable levels of Vasa even when its expression per
149 cell remained unchanged (Fig. S2O). The observations were further verified using
150 *Sod1i* localized in different chromosome to avoid any chromosome or balancer-based
151 biasness (Fig. S1G-L). However, the phenotypic effect of higher ROS was limited to
152 its origin in CySCs only because ablation of GSC redox status did not cause any
153 marked change in niche composition. *Nos-Gal4* driven knock-down of Sod1 in GSCs
154 did not result in significant change in CySC number (Fig. S2A', B' and E) but effected
155 a considerable reduction on Vasa^{+} cells (Fig. S2C', D' and F), aligning with previous
156 observations[17]. Although, Sod1 is the predominant enzyme which also localizes in the
157 intermembrane space of mitochondria, we observed a similar result upon depleting
158 the matrix localized Sod2 in both GSCs and CySCs (Fig. S2G-M), indicating
159 involvement of mitochondrial ROS for the observed cellular phenotypes.

160 To confirm active proliferation of cells and rule out the possibility of arrested growth,
161 we utilized fly- Fluorescent Ubiquitination-based Cell Cycle Indicator (FUCCI)
162 system[36] which comprises of two reporter constructs marking G1/S transition (green),
163 S (red) and G2/early mitosis (yellow) (Fig. 2H). *Tj>Sod1i* testes presented a ~2-fold
164 increase in cell number across all stages of cell-cycle (Fig 2I). The enhanced number
165 of dividing cells was contributed mainly by progressive division of CySCs, showing >2-
166 fold difference in accumulation of Zfh1^{+} nuclei in S and G2/M phases (Fig. 2J, S2PV-
167 VII and QV-VII). The number of Zfh1 labelled cells in G1/S transition was also
168 substantially more (Fig. S2PIII and QIII), indicating dysregulated redox ensued
169 increased mitotic index of CySCs. Downregulation of Sod1 in GSCs through *Nos-Gal4*
170 demonstrated no significant change in G1/S, S and G2/M phase numbers, confirming
171 our previous observation that altering ROS levels in GSCs does not have any non-
172 autonomous effect on CySCs (Fig. S2N).

173

174 **CySC induced ROS couples precocious differentiation of stem cell lineages**

175 Since, in *Sod1i* testis the number of Tj^{+} CySCs and early differentiating cells[37] were
176 elevated and more than CySC-specific Zfh1^{+} cells (Fig. 2I and J), we sought to label
177 these cells with another differentiation marker Eya (Eyes absent). We found that Eya^{+}

178 cells clustered towards the hub along with a significant increase in their number in
179 Sod1 depleted CySCs (Fig. 3A, B and D). The supposed premature expression of Eya
180 resulted in a population of differentiating cyst precursor cells co-expressing Eya-Zfh1
181 (Fig. 3A'', B'' and D). This population was found to be deviating from the normal
182 partitioning of wild type representative populations (Fig. 3C). On contrary, the same
183 cells would not show a similar phenotypical arrangement when Sod1i depletion was
184 driven in the germline lineage by *Nos-Gal4* (Fig. S3A-D). These observations hint
185 towards an obvious change in redox state of GSCs affecting their number, even when
186 generated non-autonomously from CySCs.

187 Together with reduction in Vasa^{+} GSCs shown earlier (Fig. 2G), we also detected
188 gonialblast expressing differentiation-promoting factor Bam to be much closer to the
189 hub in *Tj>Sod1i* testes (Fig. 3E'' and F''). The mean distance between the hub and
190 Bam^{+} cells was found to be shortened by ~7 microns (Fig 3G). The relative
191 advancement of spermatogonial differentiation towards the hub was also ascertained
192 by tracking the transformation of GSC-specific spectrosome into branched fusomes
193 connecting the multi-cell gonialblast (Fig. 1A). The branching fusomes were found
194 more proximal to hub than controls (Fig. 3H, I'' and J''), along with parallel reduction
195 in number of spectrosomes, implying a decline in early-stage germ cells (Fig. S3F).
196 This loss could possibly be attributed to a higher oxidizing environment in GSCs and
197 loss of intercellular contacts, particularly with hub cells (Fig. 2C# and D#). The
198 observation corroborated with decreased expression pattern of E-cadherin in *Tj>Sod1i*
199 particularly near the hub (Fig. 3K-M and S3G) and could be one of the reasons for
200 GSCs dissociation and differentiation (Fig. 2D#), due to absence of self-renewing
201 signals. Indeed, disengagement of GSCs from the hub caused reduction in Socs36E
202 and Ptp61F transcripts that act as drivers of E-cadherin expression and are induced
203 by maintenance factor STAT originating from the hub (Fig. 3N and O). These results
204 suggest that disruption of intercellular redox gradient effected premature differentiation
205 of stem cells in the niche.

206

207 **Disrupted niche architecture compromises GSC-CySC communication**

208 GSCs and CySCs intercommunicate through redox dependent factors such as EGFR,
209 PI3K/Tor to support CySC maintenance[38]. EGF ligands secreted by GSCs maintain

210 differences in cell polarity and segregates self-renewing from differentiating
211 populations[39]. *Tj>Sod1i* cells showed lower levels of cell-polarity marker Dlg (Fig. 4A",
212 B" and S4A), that expanded more into the differentiated zone (Fig. S4B). Since, Dlg
213 expression is dependent on EGFR[40], impairment in its reception was reflected in net
214 reduction in pErk levels across sections in *Sod1i* testis (Fig. S4C). Due to loss of
215 contact, this reduction was mainly limited to regions surrounding the hub, in CySC
216 zone (Fig. 4C''-D'' and E). Differentiated cyst cells presented relatively higher levels of
217 pErk expression (Fig. 4E, S4D'), particularly in *Tj>Sod1i* tissues where the pErk area
218 was significantly extended, mapping with that of Dlg (Fig. 4F) and located
219 comparatively closure to the hub (Fig. S4D), supporting its redox-dependent
220 enhancement to promote differentiation. The deregulated proliferation of cystic cells
221 reconciled with higher levels of its self-renewing inducers PI3K effector, p4E-BP (Fig.
222 4G', H' and I) and Hedgehog (Hh) (Fig. 4M' and N') [41] in *Tj>Sod1i* testis. The noticeably
223 high p4E-BP was associated with Cyclin-D accumulation (Fig. 4J). Similarly, depletion
224 of Sod1 in CySC resulted in elevated expression of Hh receptor Patched (Ptc) (Fig.
225 4O) which extended to regions farther from the hub, overlapping with expanded Tj^+
226 cells (Fig. 4M-N). Since, Ptc itself is a transcriptional Hh target, its expression in CySCs
227 suggest active Hh signalling[42], further supported by higher levels and similar pattern
228 of Hh transcriptional effector Cubitus interruptus (Ci) in *Sod1i* testis (Fig. 4P and S4E'''-
229 F'''). Since, Ptc, Ci and a GPCR-like signal transducer Smoothened (Smo) are all
230 transcriptionally driven by Hh, and Hh itself is regulated by higher levels of Ci[43,44], we
231 expectedly found higher levels of transcripts for these pathway genes (Fig. S4G-J),
232 indicating ROS-mediated upregulation of Hh activity. The overt proliferation of CySCs
233 under high ROS conditions was suppressed by reducing gene dosage either by single
234 copy of $PI3K^{DN}$ (dominant-negative allele) or Hh-RNAi (Fig. 4L and Fig. S4K-N) which
235 was also associated with an equivalent maintenance of GSC population (Fig. 4K and
236 S4O-R). Together these observations suggest that intercellular redox gradients
237 balance the stem-cell populations in the niche through CySC maintenance factors.

238

239 **Elevating CySC antioxidant defence promotes GSC self-renewal**

240 To further substantiate the role of ROS in coordinating the multi-lineage stem
241 populations, we strengthened the cellular defences against oxidants by

242 overexpressing Sod1 in CySCs and monitored the relative GSC/CySC populations.
243 Indeed, we observed an increase in the number of Vasa^{+} cells (Fig. 5A and S5A''-B''),
244 together with a slight reduction in Tj^{+} cells (Fig. 5B and S5E''-F''). Any morphological
245 anomalies associated with cell-cell adhesion or abnormal cellular dispersion, was not
246 observed (Fig. S5A-B and E-F). Enhancing the levels of Sod1 in GSCs promoted the
247 growth of GSC-like cells (Fig. S5C'', D'' and I) but did not have any prominent effect
248 on CySCs (Fig. S5G'', H'' and J). The increment in Vasa^{+} GSCs under CySC-induced
249 low redox conditions was also represented by parallel increase in spectrosome
250 number (Fig. 5C-E). The uptick in GSC number due to scavenging of ROS in CySC,
251 might be a result of delayed differentiation as indicated by displacement of Bam^{+} zone
252 away from hub; thus, confirming non-cell-autonomous role of CySC ROS in
253 maintaining GSC fate (Fig. 5F-H). The data suggest that reducing redox profile of
254 CySCs differentially affected their own self-renewing propensities along with GSC
255 maintenance and optimum redox state of both the stem-cell populations is controlled
256 by CySCs.

257

258 **Discussion:**

259 ROS is a crucial mediator of stem cell maintenance where these species act as second
260 messengers to induce different post-translational protein modifications thereby,
261 affecting cell fate[45,46]. Effectuation of ROS is mainly considered to be autocrine in
262 nature where generation of these oxidative species is compartmentalized with their
263 site of action. Recent studies have reported non-autonomous generation of ROS by
264 NOX enzymes or upon stimulation by growth factors, to play a critical role in
265 regenerative growth[47-49]. However, in either of the cases, the target cell serves as the
266 source and consequent response. Our observations in multi-lineage *Drosophila* stem
267 cell niche suggested a previously unaccounted transmission of redox signals inter-
268 cellularly that act as an organizer of niche homoeostasis. The higher ROS threshold
269 of CySCs and resultant CySC-GSC oxidative gradient maintained the physiological
270 redox state of GSC. Reduced ROS in GSC was accompanied with its proliferation[50],
271 phenocopied when Sod1 was overexpressed in its neighbours (Fig. 6).

The GSCs are attached to the hub via adherens junction to receive the maintenance signals like, Upd that trigger the JAK-STAT pathway[27,28], suppression of which activates Bam, acting as a switch from transit amplifying cells to spermatocyte differentiation[51,52]. E-cadherin levels ensure only undifferentiated stem cells to persist within the niche, while differentiating GSCs lose the competition for niche occupancy[25]. Elevated ROS in CySC possibly affected STAT phosphorylation through S-glutathionylation[53,54], causing reduced presence of dependent transcripts, Socs36E and E-cadherin thereby, resulting in detachment of GSCs from the neighbours as under E-cadherin depleted conditions[55-58]. This resulted in compromised GSC-CySC paracrine receptions such as EGFR which play a crucial role in maintenance of cell-polarity that segregates self-renewing CySC populations from the ones receiving differentiation cues [39,59,60], leading to accumulation of cells co-expressing both stemness and differentiation markers. In contrast to GSCs, ROS imbalance in CySCs induced accelerated differentiation due to deregulation of PI3K/Tor and Hedgehog pathways. Although, redox modulation of PI3K pathway components has been previously demonstrated[61], in this study we found Hedgehog to be probably susceptible to redox regulation.

However, we do not rule out the possibilities of hub cells playing an equivalent role in GSC maintenance, given their parallel effect in suppressing GSC differentiation[28]. We had tried using E-132 driver to express *Sod1i* lines in hub cells but were challenged by substantial adverse effect on fly viability. We also avoided usage of Gal80 dependent clonal populations to maintain a homogenous genetic background and prevent false readouts due to diffusion of ROS signals in unaltered neighbourhood.

The proposed concept of intercellular ROS communication can be of importance in deciphering the biochemical adaptability and plasticity of different niches influencing stem cell fate, ensuring niche size and architecture to prevent stem cell loss and aging. This has been observed in neural stem cells where inflammation-induced quiescence recovers the regenerating capacity of aging brain[62]. In addition to metabolic variations, dependence of the germline on somatic neighbours for its redox state might be one the reasons behind its presumed immortal nature and renitence to aging[63]. The same can also be applied to cancer stem cells which maintain niche occupancy and resist oxidative stress induced apoptosis probably, by receiving redox cues from the

environment. However, further work is required to elucidate the myriad of driver mechanisms intersecting at the realm of redox regulation that extend beyond the present system into broader translational areas.

Materials and Methods

Fly strains

Fly stocks were maintained and crosses were set at 25 °C on normal corn meal and yeast medium unless otherwise indicated. All fly stocks (BL-24493) *UAS SOD1 RNAi*, (BL-32909) *UAS SOD1 RNAi*, (BL-29389) *UAS SOD1 RNAi*, (BL-32983) *UAS SOD2 RNAi*, (BL-24754) *UAS SOD1*, (BL- 32489) *UAS hhRNAi*, (BL-8288) *UAS PI3K*^{DN}, (BL-25751) *UAS Dcr-nos*, (BL-55122) *UAS-FUCCI*, were obtained from Bloomington Drosophila Stock Centre. *Nos-Gal4*, *Tj-Gal4*, *Tj-Gal4-BamGFP*, *gstD1-GFP*, *TFAM-GFP* were kind gift from U. Nongthomba, P. Majumder, K. Ray, B. C. Mandal, Hong Xu labs respectively. For optimal Gal4 activity parent crosses were shifted to 29 °C till the eclosion of adults. 3-5 days old males were taken for all the experiments. The control lines for all experiments are the corresponding Gal4-line crossed with wild type *OregonR*$^{+}$.

Dissection and immunostaining

Anesthetized flies were dissected in 1X Phosphate Buffer Saline (PBS). All incubations were carried out at room temperature (25 °C) unless otherwise mentioned. Testes were fixed in 4% paraformaldehyde for 30 minutes, followed by multiple washes with 0.1% PBTX (PBS + TritonX 100). Post-blocking in 0.5% Bovine Serum Albumin, testis was incubated overnight at 4°C for primary antisera, followed by washing in 0.1% PBTX 3 times 15 minutes each before incubating with secondary antibody. The tissues were counterstained with DAPI (4,6-diamidino-2-phenylindole) for 20 minutes, followed by three washes in 0.1% PBTX 10 minutes each. For PTC staining, a modified protocol utilizing PIPES-EGTA buffer was used as described[64]. The dpErk was labelled by dissecting fly testes in Schneider's media, followed by fixation in 4% PFA for 30 min, 3x wash in 0.1% PBTX, blocked and incubated in primary antibody overnight; each step supplemented with phosphatase inhibitor cocktail 2 (1:100,

Sigma, cat#P5726). Samples were mounted in DABCO anti-fade medium prior imaging.

The following primary antibodies were used in the experiments - anti-FasIII (7G10) (1:120, DSHB (Developmental Studies Hybridoma Bank)), anti-Eya (1:50, DSHB), anti-DEcad (DCAD2) (1:50, DSHB), anti-α-Spectrin (3A9) (1:20, DSHB), anti-Ptc (1:100,DSHB) , anti-Ci (1:50, DSHB), anti-βtubulin (1:300, DSHB), anti-pERK (1:100, Cell Signaling (4370)), ATP5A (1:700, Abcam (ab14748)), anti-Tj (1:5000), anti-Vasa (1:4000), anti-Zfh1(1:2000). The primary labelling was detected using appropriate Alexa-Flour tagged secondary antibody (ThermoFisher Scientific).

To assess superoxide levels, testes were dissected in Schneider's medium (SM) and immediately incubated in 30 µM Dihydroxyethidium (DHE) at 25 °C in dark. Testes were washed thrice with SM for 7 minutes each before quantifying the emitted fluorescence using SpectraMax iD5 (Molecular Devices).

Quantitative Reverse transcription–PCR

For semi-quantitative RT-PCR and qRT-PCR analyses, total RNA was isolated from testes of 3-5 days old male flies using Qiagen RNA extraction kit. RNA pellets were resuspended in nuclease-free water and quantity of RNA was spectrophotometrically estimated. First strand cDNA was synthesized from 1-2 µg of total RNA as described earlier. The prepared cDNAs were subjected to real time PCR using forward and reverse primer pairs as listed below, using 5 µl qPCR Master Mix (SYBR Green, ThermoFisher Scientific), 2 pmol/µl of each primer per reaction for 10 µl final volume in ABI 7500 Real time PCR machine. The fold change in expression was calculated through $2^{-\Delta\Delta Ct}$ method. The primers used are listed in Supplementary Table S1.

Imaging and image analysis

Confocal imaging was carried out using Zeiss LSM 900 confocal microscope, using appropriate dichroics and filters. Images were further analyzed and processed for brightness and contrast adjustments using ImageJ (Fiji). Mean intensity measurements were carried out using standard Fiji plug-ins, 2D surface plot quantification or Zeiss Zen software as indicated. Quantification of cell number/nuclei

in single or co-stained populations (Tj, Vasa, Zfh1, Eya, FUCCI) were performed from individual slices of z-stacks using semi-automated Cell Counter plugin in Fiji for all the mentioned genotypes. The relative distance from the two reference points in the images was estimated through Inter-edge Distance ImageJ Macro v2.0 from Github. All images were assembled using Adobe Photoshop version 21.2.1.

Immunoblot Analysis

Protein was extracted from the dissected testes using RIPA buffer as described previously and quantified using Bradford reagent (Biorad). Equivalent concentration of lysate was denatured using 1X Laemelli Buffer with 1 M DTT at 95°C, separated in 10% SDS-PAGE and transferred onto PVDF membranes. Membranes were blocked with commercial blocking solution in TBST base before sequential primary antibody incubation with anti-Vasa and anti-β-Tubulin (DSHB, E7). Secondary detection was performed using HRP-tag anti-mouse antibody (GE Amersham).

Statistical analyses

All data points represent at least three biological replicates and the sample sizes carrying adequate statistical power are mentioned in the figure legends. Statistical significance for each experiment were calculated using two tailed Student's t-test unless otherwise mentioned, using GraphPad Prism 8 software. The P values were calculated through pairwise comparison of the data with wild type or driver alone and driven RNAi lines. Significance values for sample sizes mentioned in figure legends were represented as *P < 0.01, **P <0.001, or ***P < 0.0001.

Author contribution

D.S. and O.M conceived the study and designed the experiments. O.M, A.C and T.C performed the experiments. D.S and O.M analyzed the data. D.S, O.M. and A.C. wrote the manuscript.

Acknowledgements

We thank P. Majumder, U. Nongthomba, K. Ray, G. Ratnaparkhi, B. C. Mandal, Hong Xu lab and S. C. Lakhotia for kindly sharing some of the transgenic fly lines. Christian Bökel for sharing experimental protocols. Anti-Tj antibody was a generous gift from Prof. D. Godt, University of Toronto. Anti-Vasa and Anti-Zfh1 were kindly gifted by Prof. R. Lehmann, New York University. We also thank Dr. Bama Charan Mandal for generously sharing his Confocal microscope imaging system and Sudeshna Majumder for preliminary data. We acknowledge BDSC for fly stocks and DSHB for antibodies. This work is supported by Innovative Young Biotechnologist Award by Department of Biotechnology (BT/12/IYBA/2019/01), Early Career Research Award by Science and Engineering Research Board (ECR/2018/000009), BHU-Institute of Eminence grant (R/Dev/IoE/Incentive/2021-22/32452). The authors also acknowledge financial support from DST-INSPIRE fellowship (to O.M.), UGC-CAS doctoral fellowship (to T.C.).

Declaration of interest

The authors declare no competing interests

Data availability

The data that support the findings of this study are available within the main text and its Supplementary Information file. The lead contact will share all raw data associated with this paper upon request. This study did not utilize or generate any unique datasets or codes.

References

1. Schieber, M., and Chandel, N.S. (2014). ROS function in redox signaling and oxidative stress. Curr Biol *24*, R453-462. 10.1016/j.cub.2014.03.034.
2. Holmstrom, K.M., and Finkel, T. (2014). Cellular mechanisms and physiological consequences of redox-dependent signalling. Nat Rev Mol Cell Biol *15*, 411-421. 10.1038/nrm3801.
3. D'Autreaux, B., and Toledano, M.B. (2007). ROS as signalling molecules: mechanisms that generate specificity in ROS homeostasis. Nat Rev Mol Cell Biol *8*, 813-824. 10.1038/nrm2256.
4. Maryanovich, M., and Gross, A. (2013). A ROS rheostat for cell fate regulation. Trends Cell Biol *23*, 129-134. 10.1016/j.tcb.2012.09.007.
5. Murphy, M.P. (2009). How mitochondria produce reactive oxygen species. Biochem J *417*, 1-13. 10.1042/BJ20081386.

6. Hamanaka, R.B., and Chandel, N.S. (2010). Mitochondrial reactive oxygen species regulate cellular signaling and dictate biological outcomes. Trends Biochem Sci *35*, 505-513. 10.1016/j.tibs.2010.04.002.
7. Al-Mehdi, A.B., Pastukh, V.M., Swiger, B.M., Reed, D.J., Patel, M.R., Bardwell, G.C., Pastukh, V.V., Alexeyev, M.F., and Gillespie, M.N. (2012). Perinuclear mitochondrial clustering creates an oxidant-rich nuclear domain required for hypoxia-induced transcription. Sci Signal *5*, ra47. 10.1126/scisignal.2002712.
8. Bedard, K., and Krause, K.H. (2007). The NOX family of ROS-generating NADPH oxidases: physiology and pathophysiology. Physiol Rev *87*, 245-313. 10.1152/physrev.00044.2005.
9. Appenzeller-Herzog, C., Banhegyi, G., Bogeski, I., Davies, K.J., Delaunay-Moisan, A., Forman, H.J., Gorlach, A., Kietzmann, T., Laurindo, F., Margittai, E., et al. (2016). Transit of H2O2 across the endoplasmic reticulum membrane is not sluggish. Free Radic Biol Med *94*, 157-160. 10.1016/j.freeradbiomed.2016.02.030.
10. Mishina, N.M., Bogdanova, Y.A., Ermakova, Y.G., Panova, A.S., Kotova, D.A., Bilan, D.S., Steinhorn, B., Arner, E.S.J., Michel, T., and Belousov, V.V. (2019). Which Antioxidant System Shapes Intracellular H(2)O(2) Gradients? Antioxid Redox Signal *31*, 664-670. 10.1089/ars.2018.7697.
11. Yoboue, E.D., Sitia, R., and Simmen, T. (2018). Redox crosstalk at endoplasmic reticulum (ER) membrane contact sites (MCS) uses toxic waste to deliver messages. Cell Death Dis *9*, 331. 10.1038/s41419-017-0033-4.
12. Rehman, J. (2010). Empowering self-renewal and differentiation: the role of mitochondria in stem cells. J Mol Med (Berl) *88*, 981-986. 10.1007/s00109-010-0678-2.
13. Li, T.S., and Marban, E. (2010). Physiological levels of reactive oxygen species are required to maintain genomic stability in stem cells. Stem Cells *28*, 1178-1185. 10.1002/stem.438.
14. Le Belle, J.E., Orozco, N.M., Paucar, A.A., Saxe, J.P., Mottahedeh, J., Pyle, A.D., Wu, H., and Kornblum, H.I. (2011). Proliferative neural stem cells have high endogenous ROS levels that regulate self-renewal and neurogenesis in a PI3K/Akt-dependant manner. Cell Stem Cell *8*, 59-71. 10.1016/j.stem.2010.11.028.
15. Chuikov, S., Levi, B.P., Smith, M.L., and Morrison, S.J. (2010). Prdm16 promotes stem cell maintenance in multiple tissues, partly by regulating oxidative stress. Nat Cell Biol *12*, 999-1006. 10.1038/ncb2101.
16. Owusu-Ansah, E., and Banerjee, U. (2009). Reactive oxygen species prime Drosophila haematopoietic progenitors for differentiation. Nature *461*, 537-541. 10.1038/nature08313.
17. Tan, S.W.S., Lee, Q.Y., Wong, B.S.E., Cai, Y., and Baeg, G.H. (2017). Redox Homeostasis Plays Important Roles in the Maintenance of the Drosophila Testis Germline Stem Cells. Stem Cell Reports *9*, 342-354. 10.1016/j.stemcr.2017.05.034.
18. Zhou, G., Meng, S., Li, Y., Ghebre, Y.T., and Cooke, J.P. (2016). Optimal ROS Signaling Is Critical for Nuclear Reprogramming. Cell Rep *15*, 919-925. 10.1016/j.celrep.2016.03.084.
19. Sinenko, S.A., Shim, J., and Banerjee, U. (2011). Oxidative stress in the haematopoietic niche regulates the cellular immune response in Drosophila. EMBO Rep *13*, 83-89. 10.1038/embor.2011.223.
20. Davies, E.L., and Fuller, M.T. (2008). Regulation of self-renewal and differentiation in adult stem cell lineages: lessons from the Drosophila male germ line. Cold Spring Harb Symp Quant Biol *73*, 137-145. 10.1101/sqb.2008.73.063.
21. Hime, G.R., Brill, J.A., and Fuller, M.T. (1996). Assembly of ring canals in the male germ line from structural components of the contractile ring. J Cell Sci *109 (Pt 12)*, 2779-2788. 10.1242/jcs.109.12.2779.

22. Gonczy, P., and DiNardo, S. (1996). The germ line regulates somatic cyst cell proliferation and fate during Drosophila spermatogenesis. Development *122*, 2437-2447. 10.1242/dev.122.8.2437.
23. Fabrizio, J.J., Boyle, M., and DiNardo, S. (2003). A somatic role for eyes absent (eya) and sine oculis (so) in Drosophila spermatocyte development. Dev Biol *258*, 117-128. 10.1016/s0012-1606(03)00127-1.
24. Hardy, R.W., Tokuyasu, K.T., Lindsley, D.L., and Garavito, M. (1979). The germinal proliferation center in the testis of Drosophila melanogaster. J Ultrastruct Res *69*, 180-190. 10.1016/s0022-5320(79)90108-4.
25. Chen, S., Lewallen, M., and Xie, T. (2013). Adhesion in the stem cell niche: biological roles and regulation. Development *140*, 255-265. 10.1242/dev.083139.
26. Inaba, M., Yuan, H., Salzmann, V., Fuller, M.T., and Yamashita, Y.M. (2010). E-cadherin is required for centrosome and spindle orientation in Drosophila male germline stem cells. PLoS One *5*, e12473. 10.1371/journal.pone.0012473.
27. Kiger, A.A., Jones, D.L., Schulz, C., Rogers, M.B., and Fuller, M.T. (2001). Stem cell self-renewal specified by JAK-STAT activation in response to a support cell cue. Science *294*, 2542-2545. 10.1126/science.1066707.
28. Tulina, N., and Matunis, E. (2001). Control of stem cell self-renewal in Drosophila spermatogenesis by JAK-STAT signaling. Science *294*, 2546-2549. 10.1126/science.1066700.
29. Song, X., Wong, M.D., Kawase, E., Xi, R., Ding, B.C., McCarthy, J.J., and Xie, T. (2004). Bmp signals from niche cells directly repress transcription of a differentiation-promoting gene, bag of marbles, in germline stem cells in the Drosophila ovary. Development *131*, 1353-1364. 10.1242/dev.01026.
30. Kawase, E., Wong, M.D., Ding, B.C., and Xie, T. (2004). Gbb/Bmp signaling is essential for maintaining germline stem cells and for repressing bam transcription in the Drosophila testis. Development *131*, 1365-1375. 10.1242/dev.01025.
31. Losick, V.P., Morris, L.X., Fox, D.T., and Spradling, A. (2011). Drosophila stem cell niches: a decade of discovery suggests a unified view of stem cell regulation. Dev Cell *21*, 159-171. 10.1016/j.devcel.2011.06.018.
32. Jemc, J.C. (2011). Somatic gonadal cells: the supporting cast for the germline. Genesis *49*, 753-775. 10.1002/dvg.20784.
33. Zoller, R., and Schulz, C. (2012). The Drosophila cyst stem cell lineage: Partners behind the scenes? Spermatogenesis *2*, 145-157. 10.4161/spmg.21380.
34. Larsson, N.G., Wang, J., Wilhelmsson, H., Oldfors, A., Rustin, P., Lewandoski, M., Barsh, G.S., and Clayton, D.A. (1998). Mitochondrial transcription factor A is necessary for mtDNA maintenance and embryogenesis in mice. Nat Genet *18*, 231-236. 10.1038/ng0398-231.
35. Sykiotis, G.P., and Bohmann, D. (2008). Keap1/Nrf2 signaling regulates oxidative stress tolerance and lifespan in Drosophila. Dev Cell *14*, 76-85. 10.1016/j.devcel.2007.12.002.
36. Zielke, N., Korzelius, J., van Straaten, M., Bender, K., Schuhknecht, G.F.P., Dutta, D., Xiang, J., and Edgar, B.A. (2014). Fly-FUCCI: A versatile tool for studying cell proliferation in complex tissues. Cell Rep *7*, 588-598. 10.1016/j.celrep.2014.03.020.
37. Li, M.A., Alls, J.D., Avancini, R.M., Koo, K., and Godt, D. (2003). The large Maf factor Traffic Jam controls gonad morphogenesis in Drosophila. Nat Cell Biol *5*, 994-1000. 10.1038/ncb1058.
38. Amoyel, M., Hillion, K.H., Margolis, S.R., and Bach, E.A. (2016). Somatic stem cell differentiation is regulated by PI3K/Tor signaling in response to local cues. Development *143*, 3914-3925. 10.1242/dev.139782.
39. Castanieto, A., Johnston, M.J., and Nystul, T.G. (2014). EGFR signaling promotes self-renewal through the establishment of cell polarity in Drosophila follicle stem cells. Elife *3*. 10.7554/eLife.04437.

537 40. Papagiannouli, F., Berry, C.W., and Fuller, M.T. (2019). The Dlg Module and Clathrin-
538 Mediated Endocytosis Regulate EGFR Signaling and Cyst Cell-Germline Coordination
539 in the Drosophila Testis. Stem Cell Reports *12*, 1024-1040.
540 10.1016/j.stemcr.2019.03.008.
541 41. Michel, M., Kupinski, A.P., Raabe, I., and Bokel, C. (2012). Hh signalling is essential
542 for somatic stem cell maintenance in the Drosophila testis niche. Development *139*,
543 2663-2669. 10.1242/dev.075242.
544 42. Chen, Y., and Struhl, G. (1996). Dual roles for patched in sequestering and transducing
545 Hedgehog. Cell *87*, 553-563. 10.1016/s0092-8674(00)81374-4.
546 43. Chen, Y., and Struhl, G. (1998). In vivo evidence that Patched and Smoothened
547 constitute distinct binding and transducing components of a Hedgehog receptor
548 complex. Development *125*, 4943-4948. 10.1242/dev.125.24.4943.
549 44. Jiang, J., and Hui, C.C. (2008). Hedgehog signaling in development and cancer. Dev
550 Cell *15*, 801-812. 10.1016/j.devcel.2008.11.010.
551 45. Sinenko, S.A., Starkova, T.Y., Kuzmin, A.A., and Tomilin, A.N. (2021). Physiological
552 Signaling Functions of Reactive Oxygen Species in Stem Cells: From Flies to Man.
553 Front Cell Dev Biol *9*, 714370. 10.3389/fcell.2021.714370.
554 46. Liang, R., and Ghaffari, S. (2014). Stem cells, redox signaling, and stem cell aging.
555 Antioxid Redox Signal *20*, 1902-1916. 10.1089/ars.2013.5300.
556 47. Fu, X.J., Peng, Y.B., Hu, Y.P., Shi, Y.Z., Yao, M., and Zhang, X. (2014). NADPH
557 oxidase 1 and its derived reactive oxygen species mediated tissue injury and repair.
558 Oxid Med Cell Longev *2014*, 282854. 10.1155/2014/282854.
559 48. Taylor-Fishwick, D.A. (2013). NOX, NOX Who is There? The Contribution of NADPH
560 Oxidase One to Beta Cell Dysfunction. Front Endocrinol (Lausanne) *4*, 40.
561 10.3389/fendo.2013.00040.
562 49. Santabarbara-Ruiz, P., Esteban-Collado, J., Perez, L., Viola, G., Abril, J.F., Milan, M.,
563 Corominas, M., and Serras, F. (2019). Ask1 and Akt act synergistically to promote
564 ROS-dependent regeneration in Drosophila. PLoS Genet *15*, e1007926.
565 10.1371/journal.pgen.1007926.
566 50. Pan, L., Chen, S., Weng, C., Call, G., Zhu, D., Tang, H., Zhang, N., and Xie, T. (2007).
567 Stem cell aging is controlled both intrinsically and extrinsically in the Drosophila ovary.
568 Cell Stem Cell *1*, 458-469. 10.1016/j.stem.2007.09.010.
569 51. Bausek, N. (2013). JAK-STAT signaling in stem cells and their niches in Drosophila.
570 JAKSTAT *2*, e25686. 10.4161/jkst.25686.
571 52. Gonczy, P., Matunis, E., and DiNardo, S. (1997). bag-of-marbles and benign gonial
572 cell neoplasm act in the germline to restrict proliferation during Drosophila
573 spermatogenesis. Development *124*, 4361-4371. 10.1242/dev.124.21.4361.
574 53. Butturini, E., Darra, E., Chiavegato, G., Cellini, B., Cozzolino, F., Monti, M., Pucci, P.,
575 Dell'Orco, D., and Mariotto, S. (2014). S-Glutathionylation at Cys328 and Cys542
576 impairs STAT3 phosphorylation. ACS Chem Biol *9*, 1885-1893. 10.1021/cb500407d.
577 54. Xiong, Y., Uys, J.D., Tew, K.D., and Townsend, D.M. (2011). S-glutathionylation: from
578 molecular mechanisms to health outcomes. Antioxid Redox Signal *15*, 233-270.
579 10.1089/ars.2010.3540.
580 55. DeGennaro, M., Hurd, T.R., Siekhaus, D.E., Biteau, B., Jasper, H., and Lehmann, R.
581 (2011). Peroxiredoxin stabilization of DE-cadherin promotes primordial germ cell
582 adhesion. Dev Cell *20*, 233-243. 10.1016/j.devcel.2010.12.007.
583 56. Karsten, P., Hader, S., and Zeidler, M.P. (2002). Cloning and expression of Drosophila
584 SOCS36E and its potential regulation by the JAK/STAT pathway. Mech Dev *117*, 343-
585 346. 10.1016/s0925-4773(02)00216-2.
586 57. Richmond, C.A., Rickner, H., Shah, M.S., Ediger, T., Deary, L., Zhou, F., Tovaglieri,
587 A., Carlone, D.L., and Breault, D.T. (2018). JAK/STAT-1 Signaling Is Required for
588 Reserve Intestinal Stem Cell Activation during Intestinal Regeneration Following Acute
589 Inflammation. Stem Cell Reports *10*, 17-26. 10.1016/j.stemcr.2017.11.015.

590 58. Leatherman, J.L., and Dinardo, S. (2010). Germline self-renewal requires cyst stem
591 cells and stat regulates niche adhesion in Drosophila testes. Nat Cell Biol *12*, 806-811.
592 10.1038/ncb2086.
593 59. Kiger, A.A., White-Cooper, H., and Fuller, M.T. (2000). Somatic support cells restrict
594 germline stem cell self-renewal and promote differentiation. Nature *407*, 750-754.
595 10.1038/35037606.
596 60. Schulz, C., Wood, C.G., Jones, D.L., Tazuke, S.I., and Fuller, M.T. (2002). Signaling
597 from germ cells mediated by the rhomboid homolog stet organizes encapsulation by
598 somatic support cells. Development *129*, 4523-4534. 10.1242/dev.129.19.4523.
599 61. Koundouros, N., and Poulogiannis, G. (2018). Phosphoinositide 3-Kinase/Akt
600 Signaling and Redox Metabolism in Cancer. Front Oncol *8*, 160.
601 10.3389/fonc.2018.00160.
602 62. Kalamakis, G., Brune, D., Ravichandran, S., Bolz, J., Fan, W., Ziebell, F., Stiehl, T.,
603 Catala-Martinez, F., Kupke, J., Zhao, S., et al. (2019). Quiescence Modulates Stem
604 Cell Maintenance and Regenerative Capacity in the Aging Brain. Cell *176*, 1407-1419
605 e1414. 10.1016/j.cell.2019.01.040.
606 63. Snoeck, H.W. (2015). Can Metabolic Mechanisms of Stem Cell Maintenance Explain
607 Aging and the Immortal Germline? Cell Stem Cell *16*, 582-584.
608 10.1016/j.stem.2015.04.021.
609 64. Michel, M., Raabe, I., Kupinski, A.P., Perez-Palencia, R., and Bokel, C. (2011). Local
610 BMP receptor activation at adherens junctions in the Drosophila germline stem cell
611 niche. Nat Commun *2*, 415. 10.1038/ncomms1426.

612

613

614 **Figure Legends**

615 **Figure 1. Mitochondrial Distribution and Redox Profile of GSCs and CySCs in**
616 **Adult *Drosophila* Testes**

617 (A) Schematic representation of adult *Drosophila* testicular niche showing
618 arrangement of different stem cell populations (GSC – Germinal Stem Cell, CySC –
619 Cystic Stem Cell). (B-E) Differential distribution of mitochondria labelled with ATP5A
620 (green) in Vasa^{+} GSCs and Tj^{+} CySCs of wild-type fly testis; B# shows digitally zoomed
621 image of the dotted area. (F) Relative mitochondria density profile of GSCs and CySCs
622 denoted through cooccurrence of ATP5A with Tj or Vasa. A.U. - arbitrary units. (G-P)
623 Redox profiling of testicular stem cell niche using *gstD1*-GFP as intrinsic ROS reporter
624 in control (G-K) and *Tj-Gal4* driven *Sod1RNAi (Sod1i)* testis (L-P). (Q) Gaussian
625 distribution curve for the variations in *gstD1*-GFP fluorescence at CySC-GSC
626 intersection region (inset) in *Tj-Gal4* control and *Sod1i* testis. (R) Quantification of
627 mean *gstD1*-GFP fluorescence intensity (MFI) upon Sod1 knockdown represented as
628 fold change over control. Data denotes mean ± s.e.m, n = 25 (S). Colocalization
629 intensity between Vasa and *gstD1*-GFP expressed through Manders' co-localization

630 coefficient (MCC) among control and *Sod1i* cells (G). Controls are the indicated driver
631 line crossed with *Oregon R*$^{+}$. Scale bar - 10 µm. See also Figure S1.

632

633 **Figure 2. Redox disequilibrium in Cyst stem cell lineage deregulates early**
634 **CySCs and decreases the GSC number**

635 (A-B) Distribution of Tj^{+} CySC/early cyst cell around the hub (FasIII) in control and
636 driven *Sod1RNAi* testis. (C-D) Represents the rosette arrangement of Vasa^{+} GSCs
637 flanking the hub. The digitally magnified region around the hub (dotted line) as seen
638 in control (C#) and *Sod1RNAi* (D#). (E-G) Mean number of Tj^{+} cells, Zfh1^{+} early CySCs
639 and GSCs in control and *Sod1RNAi* lines shown as mean ± s.e.m, n = 10. (H)
640 Construct design of the FUCCI reporter line for tracking the cell cycle stages in
641 *Drosophila* tissues, containing degrons of Cyclin B and E2F1 proteins fused with RFP
642 or GFP. G1, S and G2/M is represented by GFP^{+}, RFP^{+} and dual labelled cells
643 respectively. (I-J) Comparative changes in the total cell population (I) or Zfh1^{+} cells (J)
644 present in G1, S and G2/M phase at the niche zone between control and *Tj>Sod1i*.
645 Data points denotes mean ± s.e.m, n = 10. Scale bar - 10 µm. See also Figure S2.

646

647 **Figure 3. ROS imbalance in CySCs promotes differentiation of both GSCs and**
648 **CySCs**

649 (A-D) Number of early CySCs (Zfh1^{+}) (A'-B'), late differentiating cyst cells (Eya^{+}) (A-
650 B) and Zfh1, Eya co-expressing population were imaged (A''-B''), represented
651 schematically (C) and quantified with respect to control and *Sod1RNAi* lines (D). Data
652 points represent mean ± s.e.m, n = 10. (E-F) The effect of Sod1 depletion in CySCs
653 on the differentiation status of GSCs as observed using *Bam-GFP* reporter line. (G)
654 The relative distance of the differentiation initiation zone (Bam^{+}) from the hub (red) in
655 control and *Sod1i* testis shown as mean ± s.e.m, n = 10. (H-J) The shape and size of
656 the spectrosomes marked with α-spectrin (green) were imaged (I''-J'') and quantified
657 for their distance from the hub (marked with asterisk) (H), n = 10. Branched fusome
658 marks differentiating populations (I'-J'). (K-L) Comparative staining of CySC-GSC
659 contacts through adherens junction using E-cadherin (monochrome/green). Dotted
660 area near the hub has been expanded as inset to show loss of E-cadherin network.

661 (M) 3D surface intensity histogram for E-cadherin expression near the hub. (N-O) Fold
662 change in expression of Stat dependent transcripts Socs36E (N) and Ptp61F (O)
663 among control and *Sod1i* niche. Data is shown as mean ± s.e.m, n = 3. Scale bar - 10
664 µm. See also Figure S3.

665

666 **Figure 4. Altered CySC redox state affects niche maintenance signals.**

667 (A-B) The expression of cell polarity marker Dlg (red) in control and *Sod1i* stem-cell
668 niche (A''-B''), (C-D) Representative image showing pErk distribution parallelly with Tj^+
669 cells and its expression pattern through Fire LUT (C''-D''). Scale bar - 10 µm. (E)
670 Segregated pErk expression patterns in CySCs near the hub and differentiating cyst
671 cells (CC), mean ± s.e.m, n = 200. (F) Estimation of the differentiation zone through
672 quantification of high pErk expressing regions. (G-I) Activation of PI3K/Tor in somatic
673 lineage was adjudged through reporter p4E-BP in *Tj>Sod1i* (G'-H') and levels of the
674 active form was quantified (I), MFI – mean fluorescence intensity shown as mean ±
675 s.e.m, n = 40. (J) Induction of Cyclin D in *Sod1i* represented as fold change over
676 controls by mean ± s.e.m, n = 3. (K-L) The number of $Vasa^+$ (K) and Tj^+ (L) cells across
677 control, *Sod1i*, *Sod1i/PI3K*^{DN} (dominant negative allele) and *Sod1i/Hhi* rescue samples
678 depicted as mean ± s.e.m, n = 10. (M'-N') Representative image showing distribution
679 of Patched (Ptc) in Tj^+ cells in control and *Tj>Sod1i*. (O-P) Quantification of Ptc (O)
680 and Hh effector Ci (P) expression through fluorescence intensity as mean ± s.e.m, n
681 (Ptc) = 90, n (Ci) = 200. See also Figure S4.

682

683 **Figure 5. Low CySC ROS sustains GSC maintenance**

684 (A-B) Bar graphs illustrating variations in $Vasa^+$ GSC (A) and Tj^+ CySCs (B) numbers
685 upon overexpressing Sod1 (*Tj>Sod*^{OE}), represented as mean ± s.e.m, n = 10. (C-E)
686 The spectrosomes labelled with α-spectrin (α-spec) were imaged (C'-D') and their
687 number was quantified (E). (F-H) The initiation of gonialblast differentiation was
688 determined by measuring the distance of Bam^+ zone from hub (red), n = 10 (F), (G''-
689 H'') shows distribution of Bam^+ reporter expressing cells. Scale bar - 10 µm. See also
690 Figure S5.

691

692 **Figure 6. Proposed role of intercellular redox gradients in GSC maintenance and**
693 **differentiation**

694 Mitochondrial abundance in GSC-CySC boundary maintains redox differential
695 between two stem cell population. Disequilibrated intercellular redox gradient
696 enhances precocious GSC differentiation and enhances CySC proliferation, thereby
697 disrupting the homeostatic balance between the two stem populations.

Figure 1

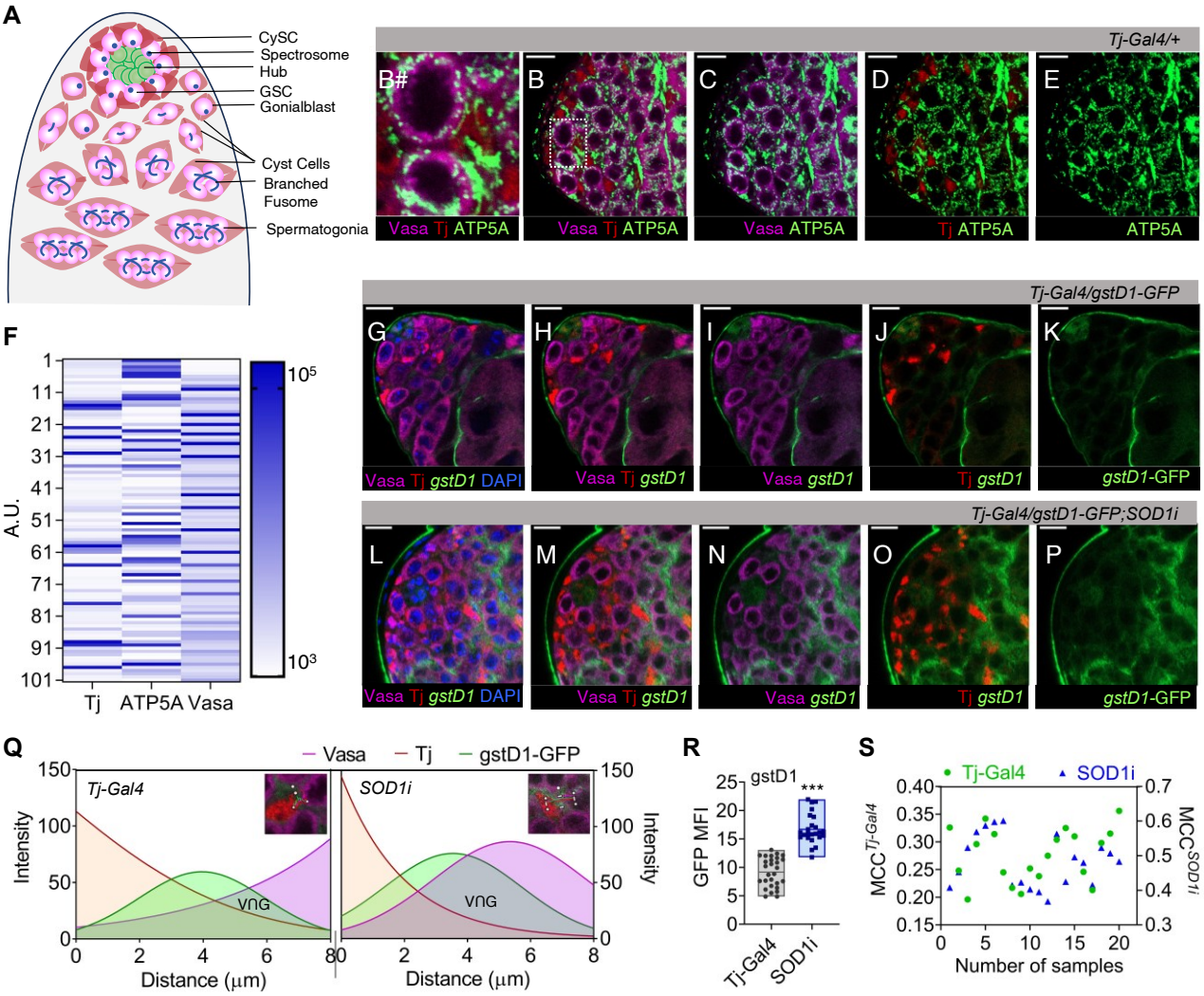
A
CySC
Spectrosome
Hub
GSC
Gonialblast
Cyst Cells
Branched Fusome
Spermatogonia
Tj-Gal4/+
B#
B
C
D
E
Vasa Tj ATP5A
Vasa Tj ATP5A
Vasa ATP5A
Tj ATP5A
ATP5A
Tj-Gal4/gstD1-GFP
G
H
I
J
K
Vasa Tj gstD1 DAPI
Vasa Tj gstD1
Vasa gstD1
Tj gstD1
gstD1-GFP
Tj-Gal4/gstD1-GFP;SOD1i
L
M
N
O
P
Vasa Tj gstD1 DAPI
Vasa Tj gstD1
Vasa gstD1
Tj gstD1
gstD1-GFP
F
A.U.
Tj
ATP5A
Vasa
Q
Vasa
Tj
gstD1-GFP
Tj-Gal4
SOD1i
VNG
Intensity
Distance (μm)
R
gstD1
GFP MFI
***
Tj-Gal4
SOD1i
S
Tj-Gal4
SOD1i
Number of samples

Figure 2

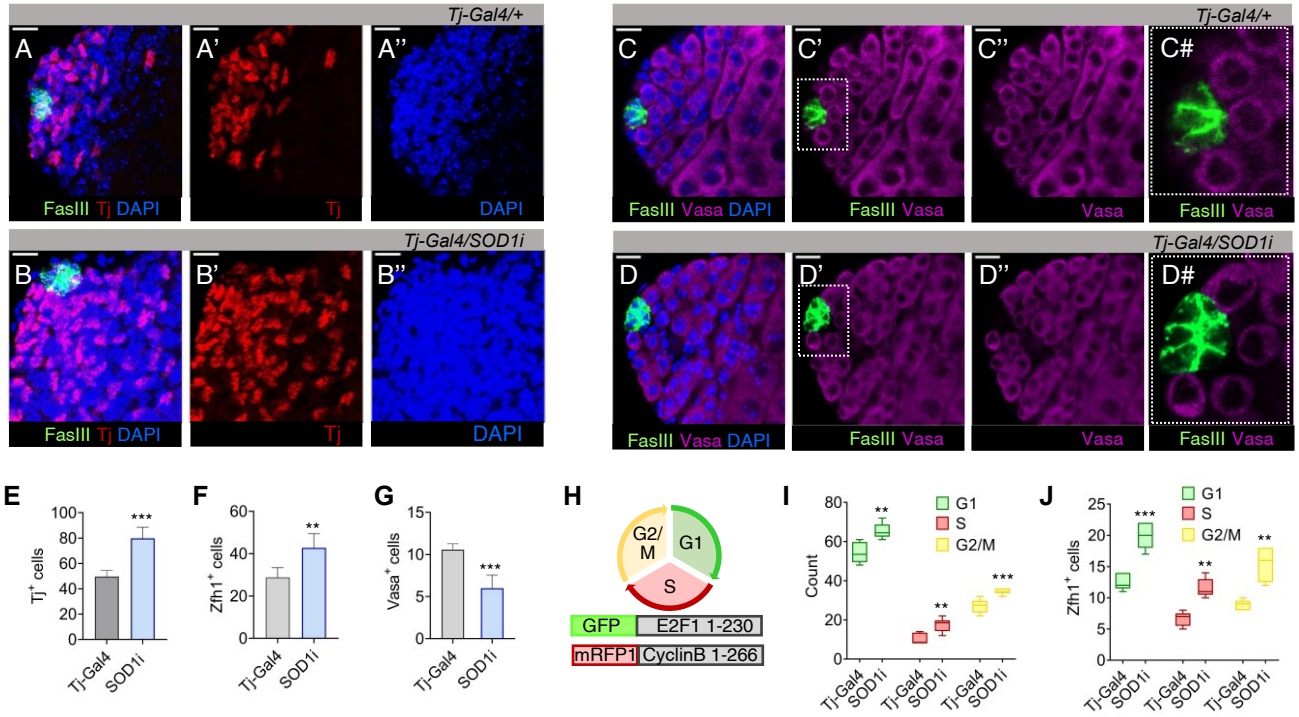
Tj-Gal4/+
A
A'
A''
FasIII Tj DAPI
Tj
DAPI
Tj-Gal4/SOD1i
B
B'
B''
FasIII Tj DAPI
Tj
DAPI
Tj-Gal4/+
C
C'
C''
C#
FasIII Vasa DAPI
FasIII Vasa
Vasa
FasIII Vasa
Tj-Gal4/SOD1i
D
D'
D''
D#
FasIII Vasa DAPI
FasIII Vasa
Vasa
FasIII Vasa
E
Tj+ cells
Tj-Gal4
SOD1i
F
Zfh1+ cells
G
Vasa+ cells
H
G2/M
G1
S
GFP
E2F1 1-230
mRFP1
CyclinB 1-266
I
Count
G1
S
G2/M
J
Zfh1+ cells

Figure 3

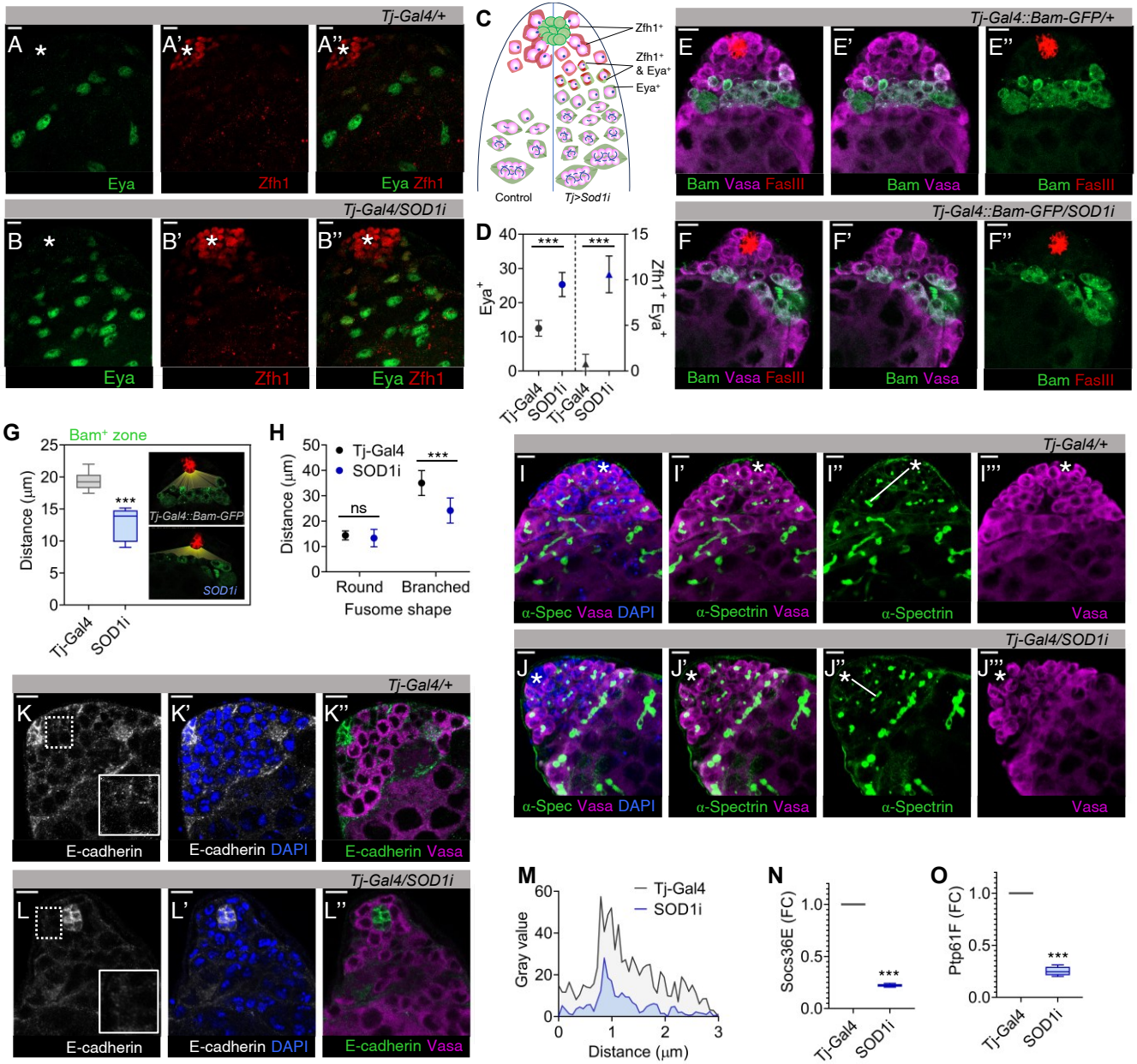
Tj-Gal4/+
A
A'
A''
Eya
Zfh1
Eya Zfh1
Tj-Gal4/SOD1i
B
B'
B''
Eya
Zfh1
Eya Zfh1
C
Zfh1+
Zfh1+ & Eya+
Eya+
Control
Tj>Sod1i
D
Eya+
Zfh1+ Eya+
Tj-Gal4
SOD1i
Tj-Gal4
SOD1i
Tj-Gal4::Bam-GFP/+
E
E'
E''
Bam Vasa FasIII
Bam Vasa
Bam FasIII
Tj-Gal4::Bam-GFP/SOD1i
F
F'
F''
Bam Vasa FasIII
Bam Vasa
Bam FasIII
G
Bam+ zone
Distance (μm)
Tj-Gal4
SOD1i
Tj-Gal4::Bam-GFP
SOD1i
H
Tj-Gal4
SOD1i
Distance (μm)
ns
Round
Branched
Fusome shape
Tj-Gal4/+
I
I'
I''
I'''
α-Spec Vasa DAPI
α-Spectrin Vasa
α-Spectrin
Vasa
Tj-Gal4/SOD1i
J
J'
J''
J'''
α-Spec Vasa DAPI
α-Spectrin Vasa
α-Spectrin
Vasa
Tj-Gal4/+
K
K'
K''
E-cadherin
E-cadherin DAPI
E-cadherin Vasa
Tj-Gal4/SOD1i
L
L'
L''
E-cadherin
E-cadherin DAPI
E-cadherin Vasa
M
Tj-Gal4
SOD1i
Gray value
Distance (μm)
N
Socs36E (FC)
Tj-Gal4
SOD1i
O
Ptp61F (FC)
Tj-Gal4
SOD1i

Figure 4

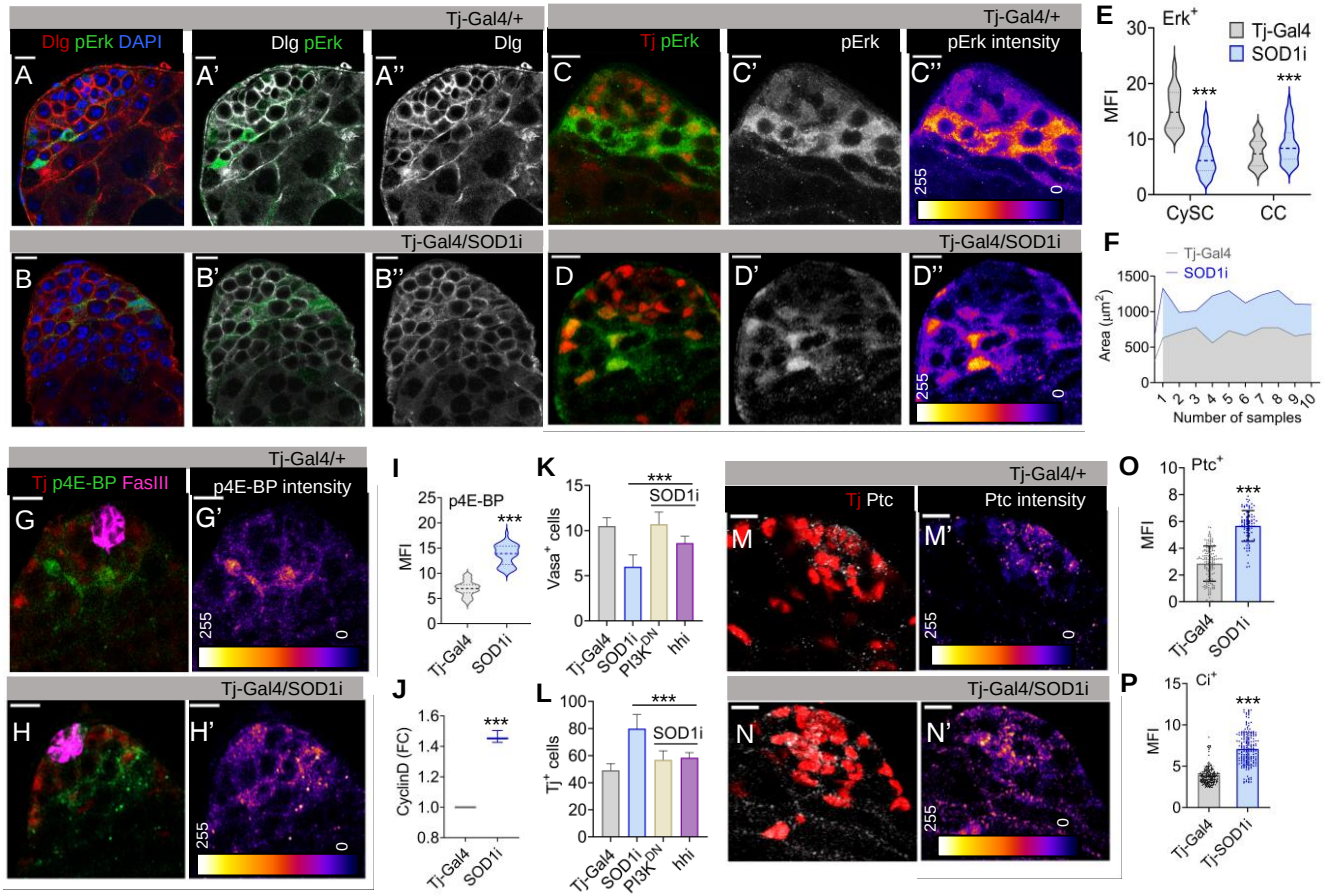
Tj-Gal4/+
Dlg pErk DAPI
Dlg pErk
Dlg
A
A'
A''
Tj pErk
pErk
pErk intensity
C
C'
C''
255
0
Tj-Gal4/SOD1i
B
B'
B''
D
D'
D''
E
Erk+
Tj-Gal4
SOD1i
MFI
***
CySC
CC
F
Tj-Gal4
SOD1i
Area (μm2)
Number of samples
Tj p4E-BP FasIII
p4E-BP intensity
G
G'
H
H'
I
p4E-BP
MFI
Tj-Gal4
SOD1i
J
CyclinD (FC)
K
Vasa+ cells
Pl3K DN
hhi
L
Tj+ cells
Tj Ptc
Ptc intensity
M
M'
N
N'
O
Ptc+
P
Ci+
Tj-SOD1i

Figure 5

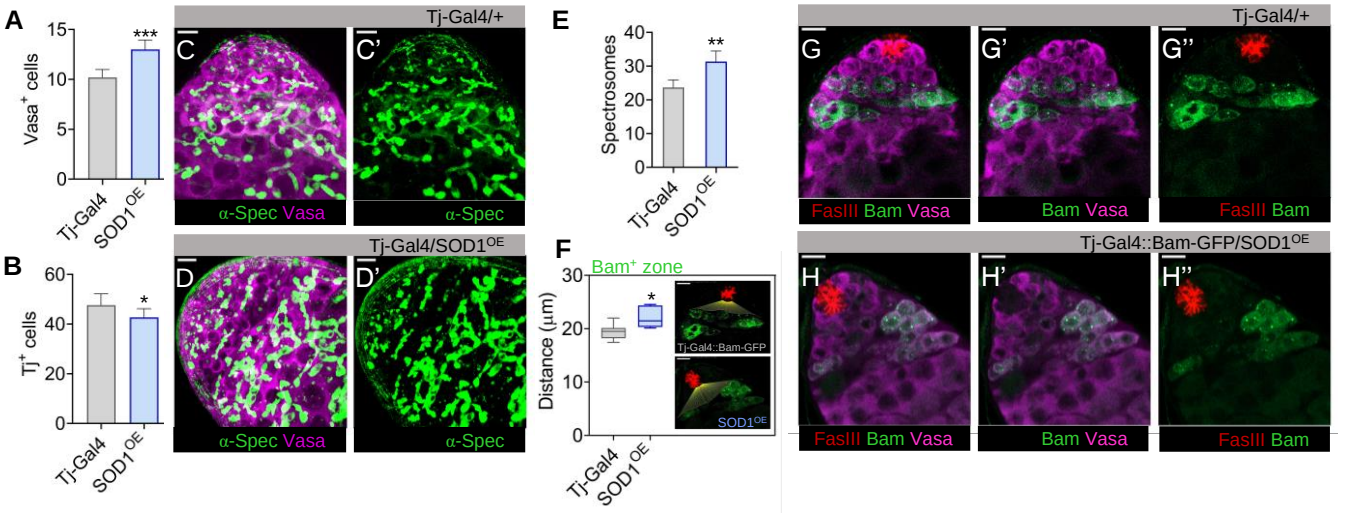
A
Vasa+ cells
15
10
5
0
***
Tj-Gal4
SOD1OE
Tj-Gal4/+
C
C'
α-Spec Vasa
α-Spec
B
Tj+ cells
60
40
20
0
*
Tj-Gal4
SOD1OE
Tj-Gal4/SOD1OE
D
D'
α-Spec Vasa
α-Spec
E
Spectrosomes
40
30
20
10
0
**
Tj-Gal4
SOD1OE
Tj-Gal4/+
G
G'
G''
FasIII Bam Vasa
Bam Vasa
FasIII Bam
F
Bam+ zone
Distance (μm)
30
20
10
0
*
Tj-Gal4
SOD1OE
Tj-Gal4::Bam-GFP
SOD1OE
Tj-Gal4::Bam-GFP/SOD1OE
H
H'
H''
FasIII Bam Vasa
Bam Vasa
FasIII Bam

Figure 6

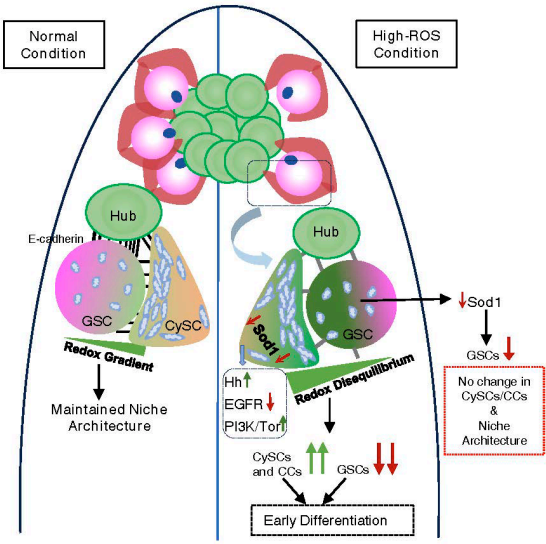
Normal Condition
High-ROS Condition
Hub
E-cadherin
GSC
CySC
Redox Gradient
Maintained Niche Architecture
Hub
Sod1
GSC
Redox Disequilibrium
Hh
EGFR
PI3K/Tor
CySCs and CCs
GSCs
Early Differentiation
Sod1
GSCs
No change in CySCs/CCs & Niche Architecture